Solar conversion of CO_2 to CO using earth-abundant electrocatalysts prepared by atomic layer modification of CuO

Marcel Schreier[1], Florent Héroguel[2], Ludmilla Steier[1], Shahzada Ahmad[3], Jeremy S. Luterbacher[2], Matthew T. Mayer[1], Jingshan Luo[1]* and Michael Grätzel[1]*

[1]Laboratory of Photonics and Interfaces, Institute of Chemical Sciences and Engineering, École Polytechnique Fédérale de Lausanne (EPFL), Lausanne, CH-1015 Switzerland

[2]Laboratory of Sustainable and Catalytic Processing, Institute of Chemical Sciences and Engineering, École Polytechnique Fédérale de Lausanne (EPFL), Lausanne, CH-1015 Switzerland

[3]Abengoa Research, Abengoa, c/Energía Solar no. 1, Campus Palmas, Altas, 41014, Sevilla, Spain

*E-mail: jingshan.luo@epfl.ch; michael.graetzel@epfl.ch

Abstract

The solar-driven electrochemical reduction of CO_2 to fuels and chemicals provides a promising way for closing the anthropogenic carbon cycle. However, the lack of selective and Earth-abundant catalysts able to achieve the desired transformation reactions in an aqueous matrix presents a substantial impediment as of today. Here we introduce atomic layer deposition of SnO_2 on CuO nanowires as a means for changing the wide product distribution of CuO-derived CO_2 reduction electrocatalysts to yield predominantly CO. The activity of this catalyst towards oxygen evolution enables us to use it both as the cathode and anode for complete CO_2 electrolysis. In the resulting device, the electrodes are separated by a bipolar membrane, allowing each half reaction to run in its optimal electrolyte environment. Using a $GaInP_2$/GaAs/Ge photovoltaic we achieve the solar driven splitting of CO_2 into CO and oxygen with a bifunctional, sustainable and all Earth-abundant system at an efficiency of 13.4%.

Introduction

The electrochemical reduction of CO_2 to fuels and chemicals has the promise to provide a versatile way of storing renewable electrical energy in chemical bonds while simultaneously closing the anthropogenic carbon cycle. A number of products have been successfully synthesized by this process, most notably carbon monoxide (CO),[1–3] formic acid (HCOOH), methane (CH_4)[4], ethylene (C_2H_4)[5] and ethanol (CH_3CH_2OH),[6] as well as other compounds .[7,8] Due to the numerous possible reaction pathways, selectively targeting one specific product at high yield has remained a challenge, which, to the present day, has only been achieved for CO and formic acid in aqueous electrolytes. Unfortunately, selective electroreduction of CO_2 to these products either relies on precious metals (Au, Ag, Pd),[9–12] requires operation at considerable overpotentials[13] or the use of electrolyte additives such as ionic liquids.[14] Developing inexpensive, selective and stable catalysts operating at low overpotentials is therefore a crucial requirement.

Recently, substantial progress toward decreasing the overpotential of copper-based electrodes was made by employing catalysts derived from copper oxides[15]. However, the insufficient selectivity remained an issue, with the catalyst producing CO, H_2 and formic acid at comparable selectivities. Following up on this work, it was demonstrated that by electrochemically reducing copper oxide in the presence of indium ions, the selectivity toward producing CO could be substantially enhanced.[16,17] More recently, the same group demonstrated tin to have a similar effect.[18] Though adding sources of metal ions during the catalyst reduction process is effective in tuning the selectivity, it is difficult to control and may not guarantee uniform coating.

Here, we demonstrate the surface modification of CuO nanowire electrodes with SnO_2 using atomic layer deposition (ALD), leading to a highly selective catalyst for the electrochemical reduction of CO_2 to CO. By using SnO_2 modified CuO nanowire electrodes in a bifunctional configuration for both the CO_2 reduction and oxygen evolution reaction (OER), we demonstrate a complete CO_2 electrolysis system that is intrinsically resistant to poisoning and uses a single Earth abundant catalyst to afford the electrochemical splitting of CO_2 into CO and oxygen. Using a triple junction $GaInP_2$/GaAs/Ge solar cell to drive the uphill reaction and a bipolar membrane as the separator we achieve the unassisted photolysis of CO_2 with a solar-to-CO free-energy conversion efficiency peaking at 13.4%. Accounting for all reduction products, the total solar to fuel efficiency (SFE) peaked at 14.4%. As solar driven CO_2 reduction to CO was achieved with one single Earth-abundant catalyst, it offers practical advantages over previously reported high-efficiency sunlight-driven CO_2 reduction systems,

where noble metal cathode materials such as gold, palladium and ruthenium have been employed along with IrO_2 to catalyse the OER.

Catalyst preparation and characterization

CuO nanowire electrodes were prepared by anodization of Cu films, followed by heat treatment. Modification with SnO_2 was carried out using atomic layer deposition, employing tetrakis(dimethylamido)tin(IV) as a metal precursor and O_3 as an oxidant.

Electron microscopy confirmed the synthesis of a nanowire structure (Figure 1a) while X-ray diffraction confirmed the presence of a crystalline CuO phase (Figure 1b), which was further confirmed by Raman spectroscopy (Figure 1c). The uniform coating with SnO_2 was observed by energy dispersive X-ray mapping (Figure 1d) and the oxidation state of Sn and Cu verified by X-ray photoelectron spectroscopy (Figure 1e-f). A detailed analysis is provided in Supplementary Note 1.

Electrochemical performance

To evaluate the catalyst's electrochemical performance for CO_2 reduction, we tested the electrodes in a Nafion-separated two-compartment cell. The electrolyte was CO_2-saturated 0.1 M $NaHCO_3$ (pH 6.75), which had been treated with an ion exchange resin (Chelex) to minimize the concentration of transition metal impurities.[19,20] Prior to polarization at the stated potential, the samples were subjected to a cathodic current of -2.0 mA cm^{-2} under CO_2 saturation to reduce the oxides until the potential reached -0.5 V vs. RHE, thereby activating the catalyst. A typical reduction curve of a CuO sample modified with 2 cycles of SnO_2 is shown in Supplementary Figure 1. Figure 2 shows the resulting electrochemical behaviour and CO_2 reduction product distribution for samples tested at different potentials. Each data point in Figure 2 a, b, c and Figure 3 a, b corresponds to the average of chronoamperometric measurements obtained from two to three independent and freshly prepared samples. Lines have been drawn as a guide to the eye and the original data are provided in Supplementary Figure 2 and 3.

As expected from the literature on copper-based catalysts, a large range of products was observed on bare CuO samples (Supplementary Figure 2).[15,21,22] CO production was found to peak at -0.6 V vs. RHE, reaching a selectivity of 36%. At lower potentials, the production of hydrogen was dominant, whereas at more negative bias, in addition to hydrogen, the

production of more reduced carbon-containing species such as ethylene, ethanol and 1-propanol was also observed.

After ALD modification with 2 pulse cycles of SnO_2, the observed current densities changed little compared to the unmodified samples (Figure 2a). At the same time, the product distribution was strongly altered (Figure 2b), which is reflected by the relative partial current densities for CO and H_2 on modified and unmodified samples (Figure 2c). With the modified samples, the dominant product was CO for all potentials, reaching a selectivity as high as 97% of all the observed products. Furthermore, even at high bias, virtually no C2 or C3 products were observed, suggesting that further reduction is inhibited in the presence of Sn. The highest yields of carbon monoxide were obtained at -0.6 V vs. RHE and a broad plateau of high CO yields was observed between -0.5 and -0.9 V vs. RHE. The sum of observed products varied between 85-100%. SnO_2-modified samples showed good stability upon extended testing as shown in Supplementary Figure 4, while 13C labelling experiments confirmed that gaseous CO_2 serves as the carbon source in this system (Supplementary Figure 5 and 6). A slight increase in CO selectivity and current density was observed upon exchanging the electrolyte cation Na^+ with K^+ and Cs^+ (Supplementary Figure 7). To account for the porous nature of the catalyst, the electrochemical surface area of SnO_2-modified and unmodified samples was determined by means of their double layer capacitance, Supplementary Figure 8. Total and partial current densities normalized to this surface area are shown in Supplementary Figure 9. Furthermore, the turnover frequencies (TOF) for CO and H_2 production have been calculated and reported in Supplementary Table 1.Note that the composition of the electrolyte also plays a role on the product selectivity, as discussed in Supplementary Note 2.

Sn and SnO_2 are known to normally lead to the production of formate as well as CO in the electrochemical reduction of CO_2.[13,23,24] We hypothesized that a cooperative effect between CuO and SnO_2 is taking place for the modified sample, altering the selectivity from what was observed on the two phases separately. To scrutinize this effect, we examined a series of CuO cathodes with different amounts of SnO_2 on the surface, testing each at a potential of -0.7 V vs. RHE (Figure 2d). It was found that maximum selectivity was achieved between 2 and 5 cycles of SnO_2, while the total current density peaked at 5 cycles. For larger cycle numbers, the selectivity for CO decreased while that of H_2 and formate increased. Similarly, the current density also decreases as the surface approaches the state of pure SnO_2 (Figure 2d). These measurements show that a specific amount of SnO_2 is required to achieve the desired effect of

modifying the product distribution to maximize the generation of CO. Large precursor doses (10 s exposure) were used to reach complete surface saturation, as described in Supplementary Figure 10. See Supplementary Note 3 for more details.

Mechanistic investigation

In Figure 3a and 3b, we analyse the formation rates of H_2 and CO, corresponding to the respective partial current densities. Due to possible sharing of catalytic sites by the HER and CO evolution reaction, the calculation of Tafel parameters lacks a theoretical basis and hence was avoided here. After modification with SnO_2, the nanowire electrodes were found to exhibit a linear trend in a plot of overpotential vs. the logarithm of the partial current density towards the production of CO. In the case of unmodified CuO nanowires, an overlapping trend could be seen in the low overpotential region, hinting at a similar mechanism for CO formation on modified and unmodified CuO nanowires. On unmodified samples, however, the production of CO substantially decreased at higher overpotentials, while the yield of H_2 and other CO_2 reduction products increased concomitantly. The production of these other products was successfully suppressed on SnO_2-modified samples, leading to a linear slope of the CO formation rate. In contrast, the production rate of H_2 was reduced by roughly an order of magnitude by the SnO_2-modified catalyst over almost the entire potential range (Figure 3a), indicating that the increased selectivity toward CO production is due to the suppression of H_2 production. We attribute the observed changes to a decrease in the adsorption strength of key reaction intermediates on the surface. To test this hypothesis experimentally, we performed chemisorption measurements.

Gas-phase adsorption measurements were carried out on CuO nanoparticle samples, reduced *in situ* under H_2, which has been shown to lead to catalytic activity comparable to that obtained by electrochemical reduction.[25,26] Particles were chosen for these measurements because their high surface area and small size are more amenable to the study in conventional chemisorption equipment. Reduction of the particles was confirmed by temperature programmed reduction (TPR, Supplementary Figure 11a) and their fluidized bed ALD modification with SnO_2 was found to lead to the same trend of selectivity changes as observed when modifying CuO nanowires (Supplementary Figure 12). The resulting adsorption isotherms, normalized to the total adsorbed gas, show that, upon modification with SnO_2, the binding strength of both CO and adsorbed hydrogen (H*) is significantly decreased (Figure 3c, 3d), as confirmed by Langmuir fits detailed in Supplementary Table 2. See also

Supplementary Note 4. Based on the volcano-relationship between hydrogen binding energy and HER performance as shown in Supplementary Figure 13a, decreasing the binding strength of H on Cu will lead to a decreased hydrogen evolution activity, in agreement with the electrochemical results observed in the previous section.[27] Furthermore, this would decrease the equilibrium concentration of H* on the catalyst surface, thereby inhibiting the further reduction of CO to alcohols and hydrocarbon species at higher bias. Interestingly, we found that for SnO_2-coated samples, the binding strength of CO was also decreased. Similar to the case of H_2, decreasing the CO binding strength of copper should shift its catalytic performance closer to that of Au and Ag, both known to be excellent catalysts for CO electrosynthesis (Supplementary Figure 13b).[8] The decreased binding strength of CO will likely also inhibit further reduction, by decreasing its surface concentration, as was observed in the partial current density analysis. Even though these results have been obtained from studies on solid-gas interfaces, they provide useful thermodynamic insight into changes in binding strength under electrochemical testing conditions, as has been proposed previously.[26] They therefore offer a plausible explanation for our observation that increased selectivity toward CO production for SnO_2 modified CuO is due to the suppression of production of H_2.

Structural change upon electrochemical testing

SnO_2 coated and uncoated nanowires had to be reduced before products were observed, indicating that the reduced form of the material constitutes the active catalyst, in agreement with earlier studies.[15,18,24] Detailed analysis of catalyst samples after electrochemical testing is provided in Supplementary Note 5. By electron energy loss spectroscopy, it is found that Cu(II) oxide is indeed reduced to the metallic form (Supplementary Figure 14), while the nanowire structure remains largely intact upon long-term testing. Furthermore, after electrolysis Sn is found to be uniformly distributed and is present mainly in the +2 oxidation state with the appearance of some Cu(I) in contrast to the initial state where Sn is mainly found as Sn(IV) at the surface. The question of whether residual oxides play a role in CO_2 reduction on oxide-derived catalysts is still under debate.[15,28–30] Furthermore, previous literature suggested that SnO_2 only led to a good performance as a CO_2 reduction catalyst when in a metastable oxide state beyond its reduction potential.[31] The oxidation states of both Sn and Cu in the active catalyst thus remain uncertain and work to address this question is being pursued.

Bifunctional catalysis

An overall electrochemical system, affecting the splitting of CO_2 into CO and O_2, requires a cathode for CO_2 reduction, an anode for water oxidation, and a membrane for product separation. Numerous Earth-abundant catalysts have been developed for the oxygen evolution reaction, most of them consisting of transition metals such as Ni and Fe, which are prone to dissolve and redeposit on the CO_2 reducing cathode. This leads to poisoning of the electrode,[19] a problem which may be averted by avoiding the use of elements foreign to the cathode. We therefore decided to investigate OER electrodes which are made from the same elements as the cathode, leading to a bifunctional catalyst configuration that has the additional benefit of making the device simpler and more cost effective. A number of recent reports have demonstrated the activity of CuO toward the oxygen evolution reaction, making it a viable bifunctional electrode for both CO_2 reduction and OER.[32–35] To assess the activity of the CuO nanowire samples for OER, linear sweep voltammetry measurements were carried out in a three-electrode setup using 0.25 M KOH as electrolyte. Oxygen evolution was observed at an overpotential of 320 mV with a current density of 0.1 mA cm^{-2}, the value being similar with and without ALD SnO_2 coating (Supplementary Figure 15a). Gas chromatography (GC) measurements confirmed quantitative oxygen evolution under these conditions, pointing to the absence of anode corrosion (Supplementary Figure 15b). However, in 1.0 M KOH, the electrode was found to rapidly deactivate. From these results we infer that SnO_2-coated CuO nanowires represent efficient catalysts for both the reduction of CO_2 to CO and the electrochemical oxidation of water to produce O_2, which enables the conception of a bifunctional system, using the same electrode for both reactions.

In contrast to the oxygen evolution reaction which is most efficient when run under alkaline conditions, electrochemical CO_2 reduction tends to work best under neutral conditions.[13] Using a catholyte that differs from the anolyte would address these problems but challenges arise from the need of using an ion exchange membrane to keep the two electrolytes apart. During operation, OH^- ions are consumed at the anode while protons are consumed at the cathode, producing a pH gradient that will ultimately arrest the reaction. At the same time, the current carrying ions are unlikely to be OH^- or H^+ since in the case of a cation exchange membrane, the positively charged electrolyte cation, present in large excess, will flow from the anode to the cathode compartment, building up a cation concentration gradient since these ions are not electroactive. A similar phenomenon would occur for anion exchange membranes, where HCO_3^- ions are to be expected to carry the current. Furthermore, passive exchange of

ions will occur across the membrane as long as their concentration is different in the two compartments.

Bipolar membranes offer an elegant solution, enabling the sustainable use of distinct electrolyte compositions, exhibiting different pH values in two separate compartments, as has been demonstrated previously for the case of water electrolysis.[36–39] This is achieved by using a double-layer membrane, consisting of an anion exchanger on the anode side and a cation exchanger on the cathode side of the cell. These block the transport of both cations and anions. Water, however, is able to penetrate between the two layers, where it is dissociated into OH^- and H^+ which are transported through their respective ion exchange layer to their respective compartment, carrying the electric current. Under these conditions, the current carrying ions consumed at the electrode in the Faradaic reactions are replenished avoiding the build-up of a pH or ion gradient, as well as avoiding passive ion exchange, as is schematically depicted in Supplementary Figure 16 and shown in Supplementary Figure 17.

Photo-driven CO_2 reduction using water as electron source

Exploiting the properties of bipolar membranes and the bifunctional nature of the SnO_2-modified CuO catalysts, we designed a 20 cm^2 prototype cell (Supplementary Figure 18) consisting exclusively of Earth-abundant materials. To optimize catalyst performance, solutions of 0.1 M $CsHCO_3$ (pH 6.75) and 0.25 M CsOH (pH 13.3) were used as catholyte and anolyte, respectively (Figure 4a and Supplementary Figure 16). The resulting dark load of the catalytic system, composed of cathode, anode and bipolar membrane, is depicted by the black curve with symbols in Figure 4b, whereas the individual potentials of the cell components as a function of the current density are depicted in Supplementary Figure 19. Unassisted solar driven CO_2 reduction was achieved using a single 3-junction $GaInP_2$/GaAs/Ge photovoltaic, as depicted in Figure 4a. The surface area of the photovoltaic cell was 0.75 cm $\times$ 0.75 cm (0.5625 cm^2), and the surface areas of the anodes and cathodes were both 20 cm^2. The device was illuminated with standard AM 1.5G solar light at room temperature and 100 mW cm^{-2} (1 sun) intensity and operated at a voltage of 2.39 V. The measured cathode potential remained constant at -0.55 V vs. RHE over the test period of 5 h and led to a solar-to-CO free energy conversion efficiency peaking at 13.4%. On average, 81% Faradaic efficiency in CO was observed and the solar-to-CO efficiency reached 12.4%, whereas the average total solar-to-fuel efficiency was found to be 13.8%. The evolution of the system potentials is shown in Supplementary Figure 20. Detailed efficiency calculations are

provided in the Methods. Overpotential losses at the anode and cathode were η_a = 380 mV and η_c = 440 mV, respectively, whereas the membrane potential was found to be 606 mV which exceeds the 370 mV potential due to the pH gradient. Over the course of the experiment, the yield in hydrogen increased slightly and concurrently with the sum of all observed products, peaking at 14.4% overall solar to fuel conversion efficiency (Supplementary Figure 21). The SFE increases to ~16% if the higher heating values of CO and H_2 are considered. The solar to CO efficiencies observed here represent a doubling in efficiency from our previous report of 6.5% for this key photo-driven CO_2 splitting reaction, which is gaining increasing attention both from academia and industry.[40]

Discussion

We introduce the use of atomic layer deposition in the field of CO_2 reduction electrocatalysis.[41] Our results show pronounced and tuneable changes in selectivity upon ALD modification of CuO. Of the 2-electron products accessible from CO_2, CO is an interesting candidate due to its gaseous character and versatility as a vector in well-established processes leading to bulk chemicals and transportation fuels.[42] In the future, direct production of reduction products such as ethylene or alcohols in an electrochemical process remains an important objective since it may provide a way to produce commodity chemicals and fuels directly from electrical power and abundant CO_2. In this context, the ability of ALD to modify the surface of CO_2 reduction catalysts with fine control of product selectivity and reproducibility is a promising and powerful tool toward the future design of CO_2 reduction catalysts. The broad range of materials accessible by ALD will likely prove particularly helpful in the framework of designing catalysts able to overcome scaling relations, which will be crucial when targeting CO_2 reduction products other than CO and HCOOH.[43]

In this report, we demonstrated an all Earth-abundant CO_2 to CO electrolyser. In addition, the SnO_2-modified CuO cathode remains selective over a large potential range, enabling stable operation at various power levels. This will become crucial for implementing solar driven fuel generating systems, where a solar to fuel catalyst must be able to tolerate light intensity fluctuations at constant selectivity. The introduction of a bipolar membrane into an electrochemical CO_2 reduction system is likely to provide a solution to the issue of maintaining pH and ion gradients, which constitutes a major issue for the field. During our tests, we found some ion crossover to occur due to imperfections of the bipolar membrane, with the percentage depending on the operating current density (Supplementary Figure 22).

Further membrane development will thus be needed to tackle this issue for sustained long term operation.

To match the maximum power output of the photovoltaic, we used catalyst electrodes with a larger surface area than the illuminated area of the photovoltaic. As the catalyst electrodes operate in the dark, they do not affect the active area of the photovoltaic that harvests solar light. Furthermore, as the electrodes are made from Earth-abundant materials, they will not increase the overall system cost much. However, this might increase the complexity of the system. Decreasing the difference in area will improve system scalability and overall system cost, which motivates continued research to improve catalyst activity.

Finally, we emphasize that deposition of ultrathin layers of SnO_2 on the surface of the catalyst led to pronounced changes in selectivity. This shows the high degree of susceptibility of CO_2 reduction catalysts to trace elements in the system, whether by design or by accident during the catalyst synthesis procedure or from impurities in the electrolyte. This sensitivity is a likely culprit for the broad variations of CO_2 reduction activity reported in the literature but at the same time also opens a large parameter space options for catalyst modifications.

In summary, we demonstrated that ALD modification of CuO nanowires with small amounts of SnO_2 successfully directs the selectivity toward producing CO in the electroreduction of CO_2. Furthermore, we have shown that the same catalyst can be applied toward the OER, which led to the design of a bifunctional, intrinsically non-poisoning and all Earth-abundant system using SnO_2-coated CuO as both CO_2 reduction and water oxidation catalyst. To allow for the sustainable operation under different catholyte and anolyte, a bipolar membrane was successfully employed. This system was driven by a 3-junction photovoltaic using simulated AM 1.5G illumination, achieving a new record solar-to-CO efficiency peaking at 13.4%. Accounting for all reduction products, the total solar to fuel efficiency peaks at 14.4%.

Methods

General. Unless stated otherwise, 18.2 MΩ water was employed and experiments were carried out in an air-conditioned room at 22 °C.

Preparation of catalyst samples. TEC 15 fluorine-doped tin oxide (FTO) glass was treated with Zn powder and 10% HCl solution to remove the conductive coating, followed by rinsing with water. Removal of the FTO layer was confirmed by the absence of electrical conductivity. Subsequently, 1.5 μm of Cu (99.995%) were deposited on the glass side of the

substrate using a DP 650 sputter coater (Alliance-Concept, France). These samples (3.3×7 cm) were subsequently anodized in 3 M KOH (technical grade, Reactolab, Switzerland).[44] The counter electrode was a sheet of FTO, coated with 500 nm of Au. Anodization was carried out at room temperature at 8 mA cm^{-2} until reaching a potential of 2 V, at which point the sample was removed and copiously rinsed with H_2O. Subsequently, the sample was left to dry on a sheet of household paper. After drying, the samples were cut to the size of 3.3 × 1 cm and dehydrated at 150 °C for 1 h in a box furnace (Lenton, UK). Heating and cooling rates were set to 10 °C min^{-1}.

ALD was carried out using a home-made ALD system that has been described in detail elsewhere.[45] SnO_2 was deposited at 118 °C from tetrakis(dimethylamino)-tin(IV) (TDMASn, 99.99% Sn, Strem Chemicals, USA). Ozone served as oxidizer and was generated by an ozone generator (AC-2025, IN USA Incorporated) supplied with oxygen (99.9995%, Carbagas, Switzerland) and producing a concentration of 13% ozone in O_2. N_2 (99.9999%, Carbagas, Switzerland) was used as carrier gas at a flow rate of 10 mln min^{-1}. Prior to deposition, the sample was pretreated with 7 × 0.01 s ozone pulses under vacuum. The precursor, heated to 65 °C was pulsed under exposure mode for 10 s, unless stated otherwise. After 15 additional seconds, the chamber was set under vacuum. After waiting for 60 s, the sample was exposed for 15 s to a 0.015 s pulse of ozone in O_2. This sequence was repeated until reaching the desired amount of cycles. Before deposition, the system was left to equilibrate for ~30 min. A constant growth/cycle of 0.15 nm/cycle was measured by ellipsometry (Sopra GES 5E) on Si wafers for depositions with Sn pulse durations of 10 s.

ALD coating of CuO nanopowders for chemisorption measurements (<50 nm, Sigma-Aldrich) was carried out using a fluidized bed ALD reactor (Beneq, Finland). Tetrakis(dimethylamino)-tin(IV) was used as precursor and H_2O as oxidizer. The precursor was held at 100 °C and deposition was carried out at 180 °C. In order to reach complete saturation with precursor, micropulsing was used. Two cycles of SnO_2 were deposited.

Powder samples were tested as follows. Ti slides (Sigma Aldrich) were etched for 1 h in boiling 1 M oxalic acid (Sigma Aldrich), followed by copious rinsing with water. 18.8 mg of nanopowder were transformed into a slurry by adding 400 µL of H_2O, followed by brief ultrasonication. Subsequently, 20 µL of this slurry were drop cast on etched Ti substrates. The non-covered area was inactivated with Kapton tape and the samples tested as described below.

Electrocatalytic testing. The non-anodized part of the 1 x 3.3 cm samples was masked with Kapton tape (Eurostat Group, France) leading to an exposed surface area between 1.6 and 2 cm^2. Subsequently, the surface area was measured and the sample was fixed in the cathode compartment of a custom-made gastight electrochemical cell (PEEK, Supplementary Figure 23), containing 15 mL of electrolyte. A membrane (Nafion 117N, Ion Power, USA), was used to separate the anode compartment, which was exposed to air. A double-junction of ceramic diaphragms (Metrohm, Switzerland) was used to separate the reference electrode (Ag/AgCl KCl sat., Metrohm, Switzerland) from the cathode compartment. Potential values were transformed to the RHE scale as follows: $V_{RHE} = V_{Ag/AgCl\ (KCl\ sat.)} + 0.197\ V + 0.059\ V \times pH$.

The electrolyte was prepared as follows. 20 g of Chelex 100 (Na-form, 100–200 mesh, Fluka, Switzerland) was added to a 0.5 M solution of $NaHCO_3$ (99+%, Sigma Aldrich), stirred for several days and stored in this form to remove transition metal impurities. Such impurities were previously shown to negatively interfere with precise CO_2 reduction studies by contaminating the cathode surface. Inductively Coupled Plasma Mass Spectrometry (ICP-MS) analysis of the resulting electrolyte found all measured impurities to be below the detection limit (Supplementary Table 3). From this stock solution, 0.1 M $NaHCO_3$ was prepared by dilution with high purity H_2O. Prior to adding to the cell, the electrolyte was sparged with CO_2 (99.998%, Carbagas, Switzerland) for several hours. Before use, the ion exchange resin was removed using a syringe filter (Filtropur S 0.2 µm, Sarsted, Germany).

A SP-300 (BioLogic, France) and an Interface 1000 (Gamry, USA) potentiostat were used to polarize the sample. Until reaching -0.5 V vs. RHE, the samples were reduced galvanostatically at -2 mA cm^{-2}, followed by polarization at the desired potential for 3 h. The resulting current was recorded every 0.5 s. For SnO_2-coated samples, samples were held at -0.7 V vs. RHE for 1 h before 6 h polarization at the desired potential.

CO_2 was sparged into the cell at 10.00 mLn min^{-1} using a mass flow controller (Bronkhorst High-Tech, F201CV, Bronkhorst, Netherlands) and at the cell outlet passed into the sample loop of a gas chromatograph (Trace ULTRA, Thermo), equipped with a ShinCarbon column (Restek, USA) and a PDD detector (Vici, USA). Helium (99.9999%, Carbagas, Switzerland) was used as carrier gas and injections were carried out approximately every 15 min. The gas analysis was calibrated using a certified gas standard containing all relevant gases in CO_2 (Carbagas, Switzerland), which was flown through the sample loop at the same flow rate as during the experiment.

Faradaic efficiencies were calculated as follows. The molar flow of gas from the test cell was calculated using the concentration of species k measured by GC (x_k [mol mol^{-1}]) and the CO_2 flow rate (F_{CO2} [mol s^{-1}]). Knowing the number of exchanged electrons to produce species k from CO_2 (n_k [-]) and the Faraday constant (96485 [C mol^{-1}]), the partial current density towards species k (i_k [A]) was calculated. Comparing the partial current density to the total current (i_{tot}) yielded the Faradaic efficiency for species k (FE_k):

$$FE_k = \frac{i_k}{i_{tot}} = \frac{x_k F_{CO_2} n_k \cdot 96485[\mathrm{C\ mol^{-1}}]}{i_{\mathrm{tot}}}$$

The data shown in Figure 2 and 3a,b derive from the chronoamperometric measurements. In order to gain insight into the reproducibility, two to three individual samples were tested in independent experiments. For unmodified samples, the average of the quantified gases and current densities from injection 3 to 11 were calculated. For SnO_2-coated samples, which were tested for a longer time, the averages from injection 6 to 22 were taken. These individual averages are shown in Supplementary Figures 5a,b,c and 6a,b,c for unmodified and modified samples, respectively, and demonstrate the good reproducibility of the catalysts. The lines in Supplementary Figures 5a,b,c and 6a,b,c correspond to the average of all the measurements taken at a given potential and are shown in Figure 2 and Figure 3a,b. The original chronoamperometric measurements of bare CuO samples and samples coated with 2 cycles of SnO_2 are shown in Supplementary Figures 2 and 3.

To substantiate that gaseous CO_2 is the source of carbon for the synthesis of carbon monoxide, experiments using isotopic $^{13}CO_2$ as reagent and $NaH^{13}CO_3$ as supporting electrolyte were carried out. The presence of ^{12}CO and ^{13}CO in the product gas was assessed by Fourier Transform Infrared (FTIR) spectroscopy of the product gas in a spectroscopic gas cell, equipped with two KBr windows. FTIR rovibrational spectra of ^{12}CO and ^{13}CO are distinct and characterized by a shift to lower wavenumbers for ^{13}CO.[46] The product gases from the electrochemical test cell were passed through the IR gas cell after residual water was condensed out at -25 °C. During a typical chronoamperometric test of a SnO_2-modified CuO sample, the substrate gas, flowing at 10mLn min^{-1}, was switched from $^{12}CO_2$ to $^{13}CO_2$. At the times indicated in Supplementary Figure 5 and 6, FTIR spectra were recorded, demonstrating the shift to the exclusive production of ^{13}CO in the presence of $^{13}CO_2$ and confirming gaseous CO_2 as the source of carbon in the reaction.

Liquid analysis was performed on the electrolyte after each polarization experiment by NMR spectroscopy using a presaturation technique to suppress the signal of water. An Avance 500 Spectrometer (Bruker, Switzerland), equipped with CryoProbe (Bruker, Switzerland) was used. 100 µL of 143 µM DMSO in D_2O were added as internal standard to 500 µL of sample in a high-field NMR tube (Wilmad Labglass, USA). In order to account for differences in T1, calibration curves were recorded for each quantified species (Supplementary Figure 24), while keeping the acquisition parameters constant for all experiments.

For liquid samples, NMR spectra were Fourier-transformed without apodization and baseline corrected using Whittaker Smoother in MestReNova. The concentration of each product was calculated from the relative peak area between DMSO, the formate singlet, ethanol triplet and 1-propanol triplet, based on calibration curves for each species. A representative NMR spectrum is shown in Supplementary Figure 25. The concentration of species *l* in the test cell (c_l [mol L^{-1}]) was multiplied with the electrolyte volume in the cell (V_{cell} [L]), the number of exchanged electrons (n_l [-]) and the Faraday constant (96485 [C mol^{-1}]) and subsequently compared to the total charge passed (q_{tot}) to yield the Faradaic efficiency (FE_l):

$$FE_l = \frac{q_l}{q_{\text{tot}}} = \frac{c_l \cdot V_{\text{cell}} \cdot n_l \cdot 96485[\text{C mol}^{-1}]}{q_{\text{tot}}}$$

The relevant potential drop for I-V correction of the Tafel plots was determined by using hybrid electrochemical impedance spectroscopy between 1 MHz and 100 mHz, 10 points/dec, 10 mV perturbation at -0.3 mA cm^{-2} in CO_2-saturated 0.1 M $NaHCO_3$ electrolyte. The measurement was carried out at the end of a test using a representive CuO nanowire sample, coated with 2 cycles of ALD SnO_2. Supplementary Figure 26 shows the resulting Nyquist curve. The IR-drop was determined to be 81 Ω.

Overpotentials were calculated as follows:

$$\eta_{CO_2/CO} = \left|E_{Cathode} - E^0_{CO_2/CO}\right|$$

$$\eta_{O_2/H2O} = \left|\mathrm{E}_{Anode} - E^0_{O_2/H2O}\right|$$

where $\eta_{CO_2/CO}$, $E_{Cathode}$, $E^0_{CO_2/CO}$ and $\eta_{O_2/H2O}$, E_{Anode}, $E^0_{O_2/H2O}$ designate the overpotentials, operating potentials of the respective electrode and themodynamic equilibrium potentials (-0.11 V vs. RHE for CO_2/CO and +1.23 V vs. RHE for O_2/H_2O) for the CO and O_2 formation half-reactions, respectively.

Solar-driven CO_2 reduction. Solar-driven CO_2 reduction experiments were carried out in a large scale prototype cell (Supplementary Figure 18), using a bipolar membrane (Fumasep FBM). 0.25 M CsOH was used as anolyte and CO_2-saturated 0.1 M $CsHCO_3$ as catholyte. Both anode and cathode were CuO nanowires, coated with 2 ALD cycles of SnO_2. The anode and cathode surface area were both 20.0 cm^2 and the membrane 10 cm^2. The system was driven using an unmasked commercial 3-junction $GaInP_2$/GaAs/Ge solar cell (Suncore, China) (Supplementary Figure 27), illuminated with a simulated AM1.5G spectrum at 1 sun intensity from an Oriel LCS-100 Class ABB solar simulator (Newport, USA) and achieving a maximum power conversion efficiency of 28.5% at 2.24 V. During operation, the potential of anode, cathode, reference electrodes in both the anode and cathode compartments and PV cell were monitored using an NI USB-6211 A/D converter and a custom-made LabView program. Before start, the cathode was activated at -0.7 V vs. RHE and then connected to the illuminated PV device together with the anode, leading to an operating current of 6.51 mA, corresponding to 0.33 mA cm^{-2} for the anode and cathode and 0.66 mA cm^{-2} for the membrane. The photocurrent density of 11.6 mA cm^{-2} is based on the illuminated surface area of the $GaInP_2$/GaAs/Ge solar cell, corresponding to 0.563 cm^2.

The solar to fuel conversion efficiency is defined by the ratio of 'chemical power out' to 'solar power in'. Specifically, for CO, it is defined by the following equation:

$$Eff_{CO} = \frac{P_{CO}}{P_{Solar}} = \frac{E^0_{CO/CO_2} \cdot J_{Solar} \cdot FE_{CO}}{P_{Solar}}$$

where P_{CO} is the power going towards the production of carbon monoxide from CO_2, P_{Solar} is the incident solar power on the solar cell, $E^0_{CO/CO_2} = 1.34\,V$ is the equilibrium potential for the reaction $CO_2 + 2e^- \rightarrow CO + \frac{1}{2} O_2$, J_{Solar} is the current density per illuminated solar absorber area and FE_{CO} is the Faradaic efficiency of CO production.

An example calculation is given as follows: Upon operation, the absolute current for CO_2 reduction was 6.51 mA. The thermodynamic potential for CO is 1.34 V. Thus, the 'chemical power out' term of our system is calculated as 6.51 mA × 1.34 V × Faradaic efficiency for CO production (FE_{CO}). On the other hand, 'solar power in' is determined by the light intensity (100 mW cm^{-2}) and the illuminated area of the absorber (0.75 cm × 0.75 cm), leading to: 100 mW cm^{-2} × 0.75 cm × 0.75 cm. As the peak Faradaic efficiency for CO production was 0.866, the peak solar to CO conversion efficiency is calculated as: 6.51 mA × 1.34 V × 0.866 / (100 mW cm^{-2} × 0.75 cm × 0.75 cm) = 13.4%.

The potential distribution in the system was measured by applying a series of currents to the cell. After stabilizing for 5 minutes at each current, the cathode and anode operating potential, as well as the membrane voltage were recorded against Ag/AgCl reference electrodes in each compartment. The resulting potential distribution is shown in Supplementary Figure 19.

Sample characterization. X-Ray diffraction was carried out on a D8 DISCOVER diffractometer (Bruker, Germany), equipped with a silicon strip detector LynxEye (Bruker, Germany) and a monochromated Cu K-α source. Patterns were recorded in locked-coupled mode between $2\theta = 10$ to 70°, at 0.1° min^{-1} with a step size of 0.02.

Raman scattering experiments were carried out using an XploRA ONE Raman microscope (Horiba, Japan), equipped with a 532 nm doubled Nd:YAG DPSS laser. The laser power was set to 25%, acquisition time was 3 s and 200 spectra were recorded for each sample. X-Ray photoelectron spectroscopy and profile analysis was carried out using a PHI VersaProbe II XPS microprobe. Scanning electron microscopy was carried out on a MERLIN high resolution SEM (Zeiss, Germany).

Transmission electron microscopy was carried out on a Technai Osiris electron microscope (FEI), and elemental mappings were obtained from energy-dispersive X-ray (EDX) spectra obtained in scanning transmission electron microscopy (STEM) mode. Aberration-corrected STEM was carried out on a Titan Themis (FEI).

Volumetric measurements of H_2 and CO adsorption isotherms were carried out at 35 °C between 2 and 300 mbar on a Micromeritics 3 Flex instrument. The sample (300 mg) was loaded into a U-shaped cell and reduced in-situ under H_2 flow (50 mL $min^{-1)}$ at 250 °C (5 °C min^{-1}) for 1 h and adsorbed H_2 was removed by vacuum (< 10^{-3} mbar) at 250 °C for 30 min. After cooling down to 35 °C under vacuum, a leak test was performed prior to analysis.

H_2 Temperature programmed reduction (H_2-TPR) experiments were carried out on a Micromeritics Autochem 2920 instrument. The sample (300 mg) was loaded into a U-shaped cell and dried under He flow (50 mL min^{-1}) at 120 °C (5 °C min^{-1}) for 30 min. After cooling down to 40 °C, the flow was switched to a H_2/Ar mixture (10/90 vol.) and the sample was ramped to 250 °C (10 °C min^{-1}) while H_2 consumption was quantified using a calibrated thermal conductivity detector (TCD). An isopropanol/liquid N_2 cold bath was used between the sample and the TCD to trap water produced during TPR, the absence of which was verified by monitoring mass 18 on a MKS Cirrus 2 mass spectrometer placed after the TCD.

Inductively Coupled Plasma Mass Spectrometry (ICP-MS) measurements were carried out on a Perkin-Elmer DRC II. A plasma torch in axial position was run under argon 99.99998%. Calibration was carried on each of the measured elements between 1 and 50 µg/l over 6 points. Prior to analysis, samples were diluted 10'000 times in order to avoid saturation due to excess sodium ions from the electrolyte.

Bipolar membrane characterization was carried out by running a 10 cm^2 bipolar membrane using two Pt wire electrodes with CO_2-saturated 0.1 M $CsHCO_3$ catholyte and 0.25 M CsOH anolyte at various current densities until reaching ~125 Coulombs of passed charge. Electrolyte composition analysis of the initial and final state was subsequently performed by ion chromatography using a Dionex Integrion HPIC System (Thermo Fisher Scientific). Samples were diluted 100x with water in order to avoid saturation.

The electrochemical surface area was determined by cyclic voltammetry on previously tested samples (Supplementary Figure 8). Measurements were carried out in a pH 5 phosphate buffer containing 0.1 M phosphate and 0.5 M Na_2SO_4. Data were recorded between -0.3 and -0.2 V vs. Ag/AgCl (KCl sat.) at 100 mV sec^{-1} to 10 mV sec^{-1} in 10 mV sec^{-1} steps. To determine the capacitance, half the difference between the positive and negative sweep were taken at -0.25 V vs. Ag/AgCl and a linear fit was carried out, the slope of which corresponds to the capacitance. Comparing the capacitance of flat Cu sputtered on glass with the capacitance of an unmodified CuO nanowire sample and one modified with 2 ALD cycles of SnO_2, yielded a roughness factor of 17.26 and 17.28, respectively. Atomic Force Microscopy (AFM) measurements of sputtered Cu on glass using a "Cypher" AFM device from Asylum Research determined its roughness factor to be 1.004, yielding a total roughness factor of 17.33 and 17.34, respectively, and indicating that no significant difference in roughness between SnO_2 modified and unmodified samples exists. Current densities relative to the entire surface area are shown in Supplementary Figure 8.

The turnover frequency (TOF), shown in Supplementary Table 1 and in Supplementary Figure 9b, was calculated using the roughness factor and the surface atom density of copper. Based on a previous report,[7] the surface atom density of Cu(111) of 3.155×10^{-3} µmol cm^{-2} was used. The rates of formation of CO and H_2 were normalized to the amount of surface atoms, leading to the reported turnover frequencies at different overpotentials.

Data availability statement

The data that support the plots within this paper and other findings of this study are available from the corresponding author upon reasonable request.

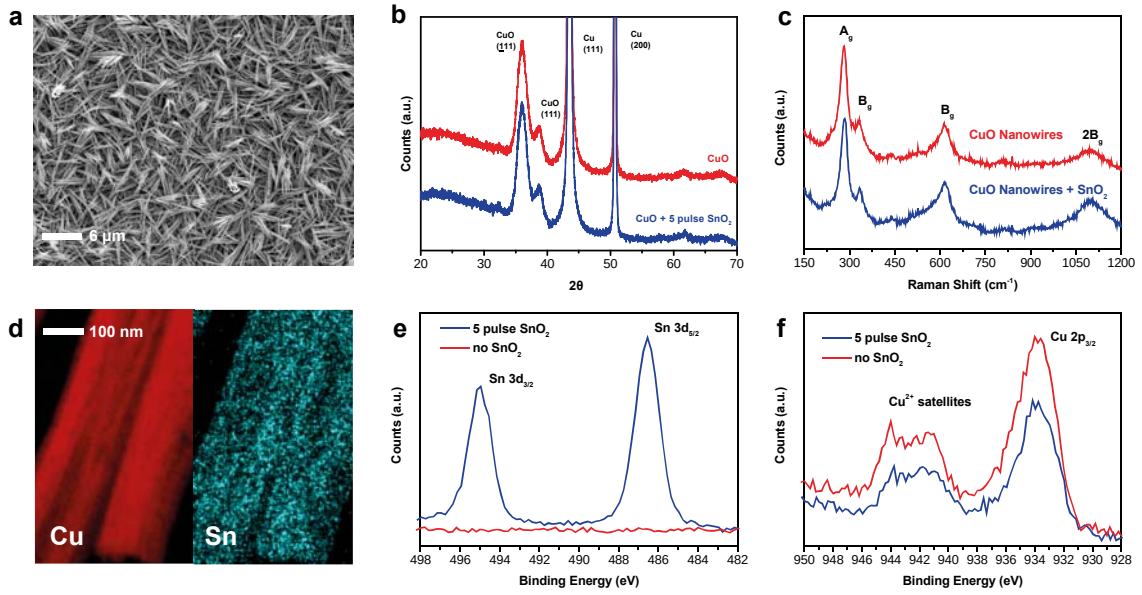

528

529 **Figure 1 | Structural and compositional characterizations of CuO nanowires with and without**
530 **SnO_2 surface modification. a,** SEM micrograph of as-prepared CuO nanowires. **b,** X-Ray diffraction
531 pattern of SnO_2-modified and unmodified samples. From the annotated reflections, the presence of
532 CuO can be observed but no reflections corresponding to SnO_2 were detected. **c,** Raman spectrum of
533 SnO_2-modified and unmodified samples. The characteristic modes of CuO were observed; however,
534 no modes relative to SnO_2 were detected. **d,** STEM-EDX mapping of a CuO nanowire after coating
535 with 5 ALD cycles of SnO_2. Sn is uniformly distributed on the nanowire. **e,** Sn 3d XPS spectrum,
536 confirming the presence of Sn after modification of CuO nanowire samples with 5 cycles of SnO_2. **f,**
537 Cu 2p XPS spectrum, showing the features of Cu^{2+} satellites, which confirm the presence of CuO.

538

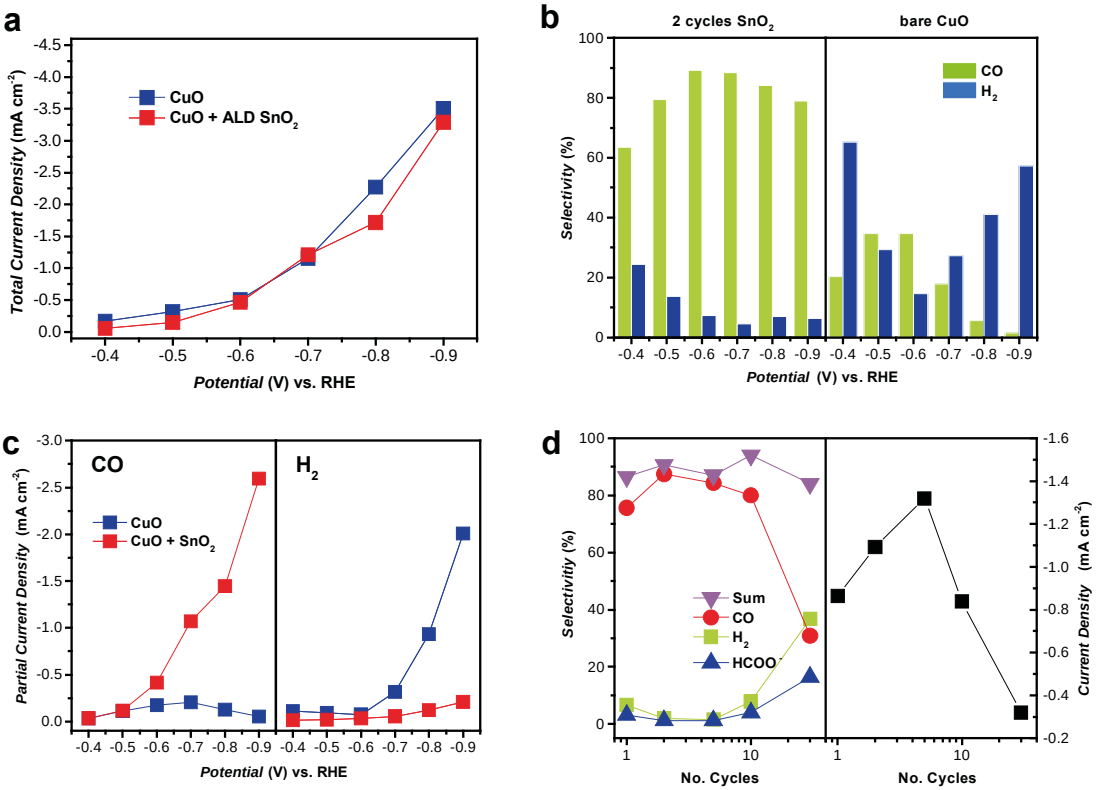

Figure 2 | Electrochemical CO_2 reduction performance. a, Current densities of SnO_2-modified and unmodified samples derived from chronoamperometric measurements. **b,** Faradaic selectivity toward CO and H_2 for samples modified with 2 ALD cycles of SnO_2 (left) and for unmodified samples (right). **c,** Partial current densities toward CO (left) and H_2 (right) from SnO_2-modified samples (2 ALD cycles) and unmodified samples derived from chronoamperometric measurements. **d,** Impact of the amount of deposited SnO_2 (by ALD cycles) on the electrocatalytic performance and selectivity at -0.7 V vs. RHE. Current densities have been calculated using the geometric surface area of the samples. The chronoamperometric measurements for a, b and c are presented in Supplementary Figures 5 and 6. Lines have been drawn as a guide to the eye and the current densities are based on the geometric surface area.

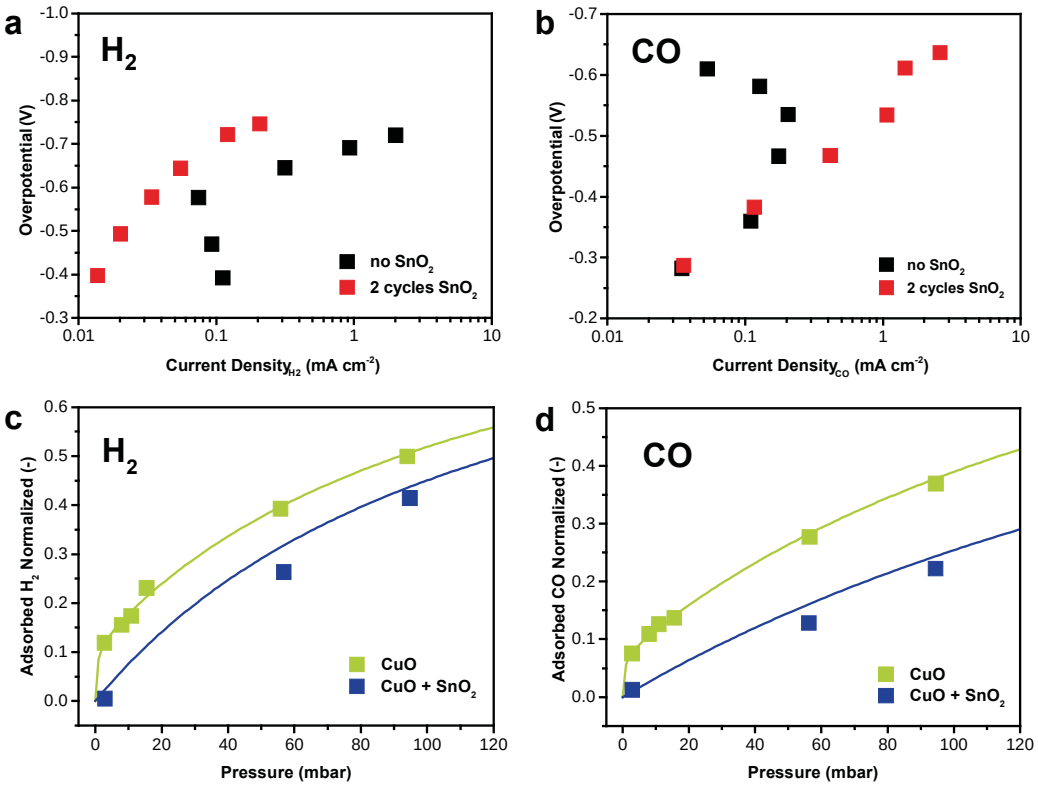

550

551 **Figure 3 | Partial current density and chemisorption analysis.** IR-corrected logarithmic plots of the
552 current densities for (**a**) H_2 and (**b**) CO from SnO_2-modified (2 ALD cycles) and unmodified CuO
553 nanowire samples. Chemisorption measurements for (**c**) H_2 and (**d**) CO from SnO_2-modified (2 ALD
554 cycles) and unmodified CuO nanopowder. The solid lines correspond to the Langmuir fit of the data.
555 For better comparison of affinities, the data has been normalized to the quantity adsorbed at saturation
556 (S_0), as obtained from Langmuir fits.

557

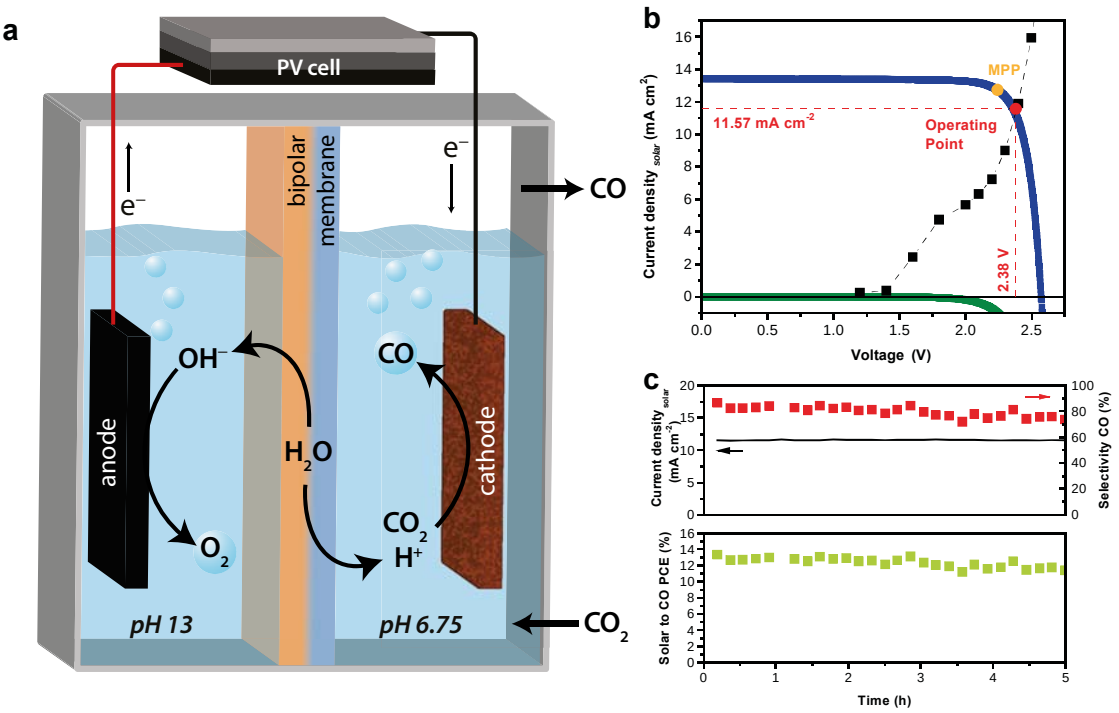

Figure 4 | Photoelectrolysis of CO_2. a, Schematic of the solar-driven CO_2 reduction device. The following reactions take place. Anode: $2\ OH^- \rightarrow H_2O + ½\ O_2 + 2e^-$, Cathode: $CO_2 + 2\ H^+ + 2\ e^- \rightarrow CO + H_2O$. The illuminated surface area of the photovoltaic cell is 0.75 cm×0.75 cm (0.5625 cm^2), the surface area of anode and cathode are both 20 cm^2, and the membrane area is 10 cm2. **b,** Photovoltaic and electrocatalytic J-V behaviors. The photovoltaic performance is shown under light (blue) and in the dark (green) and its maximum power point (MPP, 28.5%) has been marked by a yellow dot. The measured operating current density of the CO_2 electrolysis system (cathode, anode and bipolar membrane) at different voltages has been marked by black squares. The black dashed lines serve as a guide to the eye. The observed long term operating point of solar driven CO_2 electrolysis is marked by a red dot, with the red dashed lines showing the corresponding current density and voltage. We observed good agreement between the calculated intersection and the measured operating point for the device. **c,** Selectivity toward carbon monoxide, solar current density and solar-to-CO efficiency as a function of photoelectrolysis time.

References

1. Schreier, M. *et al.* Efficient and selective carbon dioxide reduction on low cost protected Cu_2O photocathodes using a molecular catalyst. *Energy Env. Sci* **8,** 855–861 (2015).

2. Schreier, M. *et al.* Covalent Immobilization of a Molecular Catalyst on Cu2O Photocathodes for CO2 Reduction. *J. Am. Chem. Soc.* **138,** 1938–1946 (2016).
3. Lau, G. P. S. *et al.* New Insights Into the Role of Imidazolium-Based Promoters for the Electroreduction of CO_2 on a Silver Electrode. *J. Am. Chem. Soc.* **138,** 7820–7823 (2016).
4. Zhang, S. *et al.* Polymer-supported CuPd nanoalloy as a synergistic catalyst for electrocatalytic reduction of carbon dioxide to methane. *Proc. Natl. Acad. Sci.* **112,** 15809–15814 (2015).
5. Ren, D. *et al.* Selective Electrochemical Reduction of Carbon Dioxide to Ethylene and Ethanol on Copper(I) Oxide Catalysts. *ACS Catal.* **5,** 2814–2821 (2015).
6. Qiao, J., Liu, Y., Hong, F. & Zhang, J. A review of catalysts for the electroreduction of carbon dioxide to produce low-carbon fuels. *Chem. Soc. Rev.* **43,** 631 (2014).
7. Kuhl, K. P., Cave, E. R., Abram, D. N. & Jaramillo, T. F. New insights into the electrochemical reduction of carbon dioxide on metallic copper surfaces. *Energy Environ. Sci.* **5,** 7050–7059 (2012).
8. Kuhl, K. P. *et al.* Electrocatalytic Conversion of Carbon Dioxide to Methane and Methanol on Transition Metal Surfaces. *J. Am. Chem. Soc.* **136,** 14107–14113 (2014).
9. Chen, Y., Li, C. W. & Kanan, M. W. Aqueous CO2 Reduction at Very Low Overpotential on Oxide-Derived Au Nanoparticles. *J. Am. Chem. Soc.* **134,** 19969–19972 (2012).
10. Feng, X., Jiang, K., Fan, S. & Kanan, M. W. Grain-Boundary-Dependent CO2 Electroreduction Activity. *J. Am. Chem. Soc.* **137,** 4606–4609 (2015).
11. Min, X. & Kanan, M. W. Pd-Catalyzed Electrohydrogenation of Carbon Dioxide to Formate: High Mass Activity at Low Overpotential and Identification of the Deactivation Pathway. *J. Am. Chem. Soc.* **137,** 4701–4708 (2015).
12. Lu, Q. *et al.* A selective and efficient electrocatalyst for carbon dioxide reduction. *Nat. Commun.* **5,** (2014).
13. Hori, Y. in *Handbook of Fuel Cells* (John Wiley & Sons, Ltd, 2010).

14. DiMeglio, J. L. & Rosenthal, J. Selective Conversion of CO2 to CO with High Efficiency Using an Inexpensive Bismuth-Based Electrocatalyst. *J. Am. Chem. Soc.* **135,** 8798–8801 (2013).
15. Li, C. W. & Kanan, M. W. CO2 Reduction at Low Overpotential on Cu Electrodes Resulting from the Reduction of Thick Cu2O Films. *J. Am. Chem. Soc.* **134,** 7231–7234 (2012).
16. Rasul, S. *et al.* A Highly Selective Copper–Indium Bimetallic Electrocatalyst for the Electrochemical Reduction of Aqueous CO2 to CO. *Angew. Chem. Int. Ed.* **54,** 2146–2150 (2015).
17. Watanabe, M., Shibata, M., Kato, A., Azuma, M. & Sakata, T. Design of Alloy Electrocatalysts for CO 2 Reduction III . The Selective and Reversible Reduction of on Cu Alloy Electrodes. *J. Electrochem. Soc.* **138,** 3382–3389 (1991).
18. Sarfraz, S., Garcia-Esparza, A. T., Jedidi, A., Cavallo, L. & Takanabe, K. Cu–Sn Bimetallic Catalyst for Selective Aqueous Electroreduction of CO_2 to CO. *ACS Catal.* **6,** 2842–2851 (2016).
19. Wuttig, A. & Surendranath, Y. Impurity Ion Complexation Enhances Carbon Dioxide Reduction Catalysis. *ACS Catal.* **5,** 4479–4484 (2015).
20. Lum, Y. *et al.* Trace Levels of Copper in Carbon Materials Show Significant Electrochemical CO_2 Reduction Activity. *ACS Catal.* **6,** 202–209 (2016).
21. Gattrell, M., Gupta, N. & Co, A. A review of the aqueous electrochemical reduction of CO2 to hydrocarbons at copper. *J. Electroanal. Chem.* **594,** 1–19 (2006).
22. Ma, M., Djanashvili, K. & Smith, W. A. Selective electrochemical reduction of CO_2 to CO on CuO-derived Cu nanowires. *Phys Chem Chem Phys* **17,** 20861–20867 (2015).
23. Chen, Y. & Kanan, M. W. Tin Oxide Dependence of the CO_2 Reduction Efficiency on Tin Electrodes and Enhanced Activity for Tin/Tin Oxide Thin-Film Catalysts. *J. Am. Chem. Soc.* **134,** 1986–1989 (2012).
24. Zhang, S., Kang, P. & Meyer, T. J. Nanostructured Tin Catalysts for Selective Electrochemical Reduction of Carbon Dioxide to Formate. *J. Am. Chem. Soc.* **136,** 1734–1737 (2014).
25. Li, C. W., Ciston, J. & Kanan, M. W. Electroreduction of carbon monoxide to liquid fuel on oxide-derived nanocrystalline copper. *Nature* **508,** 504–507 (2014).

627 26. Verdaguer-Casadevall, A. *et al.* Probing the Active Surface Sites for CO Reduction on Oxide-
628 Derived Copper Electrocatalysts. *J. Am. Chem. Soc.* **137,** 9808–9811 (2015).
629 27. Nørskov, J. K. *et al.* Trends in the Exchange Current for Hydrogen Evolution. *J. Electrochem. Soc.*
630 **152,** J23 (2005).
631 28. Eilert, A., Roberts, F. S., Friebel, D. & Nilsson, A. Formation of Copper Catalysts for CO_2 Reduction
632 with High Ethylene/Methane Product Ratio Investigated with In Situ X-ray Absorption
633 Spectroscopy. *J. Phys. Chem. Lett.* **7,** 1466–1470 (2016).
634 29. Lee, S., Kim, D. & Lee, J. Electrocatalytic Production of C3-C4 Compounds by Conversion of CO_2
635 on a Chloride-Induced Bi-Phasic Cu_2O-Cu Catalyst. *Angew. Chem. Int. Ed.* **54,** 14701–14705
636 (2015).
637 30. Mistry, H. *et al.* Highly selective plasma-activated copper catalysts for carbon dioxide reduction
638 to ethylene. *Nat. Commun.* **7,** 12123 (2016).
639 31. Dutta, A., Kuzume, A., Rahaman, M., Vesztergom, S. & Broekmann, P. Monitoring the Chemical
640 State of Catalysts for CO_2 Electroreduction: An In Operando Study. *ACS Catal.* **5,** 7498–7502
641 (2015).
642 32. Deng, Y., Handoko, A. D., Du, Y., Xi, S. & Yeo, B. S. *In Situ* Raman Spectroscopy of Copper and
643 Copper Oxide Surfaces during Electrochemical Oxygen Evolution Reaction: Identification of Cu^{III}
644 Oxides as Catalytically Active Species. *ACS Catal.* **6,** 2473–2481 (2016).
645 33. Liu, X., Cui, S., Qian, M., Sun, Z. & Du, P. In situ generated highly active copper oxide catalysts for
646 the oxygen evolution reaction at low overpotential in alkaline solutions. *Chem Commun* **52,**
647 5546–5549 (2016).
648 34. Liu, X. *et al.* Self-Supported Copper Oxide Electrocatalyst for Water Oxidation at Low
649 Overpotential and Confirmation of Its Robustness by Cu K-Edge X-ray Absorption Spectroscopy. *J.*
650 *Phys. Chem. C* **120,** 831–840 (2016).

35. Liu, X. *et al.* Nanostructured copper oxide electrodeposited from copper(II) complexes as an active catalyst for electrocatalytic oxygen evolution reaction. *Electrochem. Commun.* **46,** 1–4 (2014).
36. Luo, J. *et al.* Bipolar Membrane-Assisted Solar Water Splitting in Optimal pH. *Adv. Energy Mater.* (2016). doi:10.1002/aenm.201600100
37. Vargas-Barbosa, N. M., Geise, G. M., Hickner, M. A. & Mallouk, T. E. Assessing the Utility of Bipolar Membranes for use in Photoelectrochemical Water-Splitting Cells. *ChemSusChem* **7,** 3017–3020 (2014).
38. Vermaas, D. A., Sassenburg, M. & Smith, W. A. Photo-assisted water splitting with bipolar membrane induced pH gradients for practical solar fuel devices. *J Mater Chem A* **3,** 19556–19562 (2015).
39. Sun, K. *et al.* A Stabilized, Intrinsically Safe, 10% Efficient, Solar-Driven Water-Splitting Cell Incorporating Earth-Abundant Electrocatalysts with Steady-State pH Gradients and Product Separation Enabled by a Bipolar Membrane. *Adv. Energy Mater.* (2016). doi:10.1002/aenm.201600379
40. Schreier, M. *et al.* Efficient photosynthesis of carbon monoxide from CO2 using perovskite photovoltaics. *Nat. Commun.* **6,** 7326 (2015).
41. O'Neill, B. J. *et al.* Catalyst Design with Atomic Layer Deposition. *ACS Catal.* **5,** 1804–1825 (2015).
42. Dry, M. E. The Fischer–Tropsch process: 1950–2000. *Catal. Today* **71,** 227–241 (2002).
43. Li, Y. & Sun, Q. Recent Advances in Breaking Scaling Relations for Effective Electrochemical Conversion of CO_2. *Adv. Energy Mater.* (2016). doi:10.1002/aenm.201600463
44. Luo, J. *et al.* Cu2O Nanowire Photocathodes for Efficient and Durable Solar Water Splitting. *Nano Lett.* **16,** 1848–1857 (2016).
45. Steier, L. *et al.* Low-Temperature Atomic Layer Deposition of Crystalline and Photoactive Ultrathin Hematite Films for Solar Water Splitting. *ACS Nano* **9,** 11775–11783 (2015).

46. Tidwell, E. K. P., Lamdin R.Blaine, Eugene D. Infrared absorption and emission spectra of carbon monoxide in the region from 4 to 6 microns. *J. Res. Natl. Bur. Stand.* **55,** 183 (1955).

Acknowledgements

Thanks go to Mr Linfeng Pan for experimental help during revision, Karine Vernez Thomas and Sylvain Coudret for ICP-MS analysis, to Pierre Mettraux for XPS analysis, to Mikko Söderlund and Hugo Tholense (Beneq, Finland) for FBR-ALD depositions and to Dr. Duncan Alexander for Aberration Corrected STEM data. This work was funded by Siemens AG, and M.S. and M.G. would like to express their particular gratitude to Siemens AG for continued support. Ji.L. acknowledges Marie Skłodowska-Curie Fellowship from the European Union's Seventh Framework Programme for research, technological development and demonstration under grant agreement no 291771 for financial support.

Author contributions

M.S. designed the project, prepared samples, conducted experiments, analyzed the data and wrote the manuscript. Ji.L. designed and supervised the project, contributed to experiments, writing of the manuscript as well as to data analysis. F.H. conducted chemisorption and TPD measurements and analyzed the relevant data. L.S. assisted with ALD deposition of SnO_2. Je.L. assisted with chemisorption and TPD analysis and corrected the manuscript. M.T.M. contributed to writing the manuscript. S.A provided the 3-junction solar cells. M.G. supervised the project, directed the research and established the final version of the manuscript. All authors commented on the paper.

Additional Information

Supplementary information is available online. Reprints and permissions information is available online at www.nature.com/reprints. Correspondence and requests for materials should be addressed to M.G. or Ji.L.

Competing interests

The authors declare no competing financial interests.

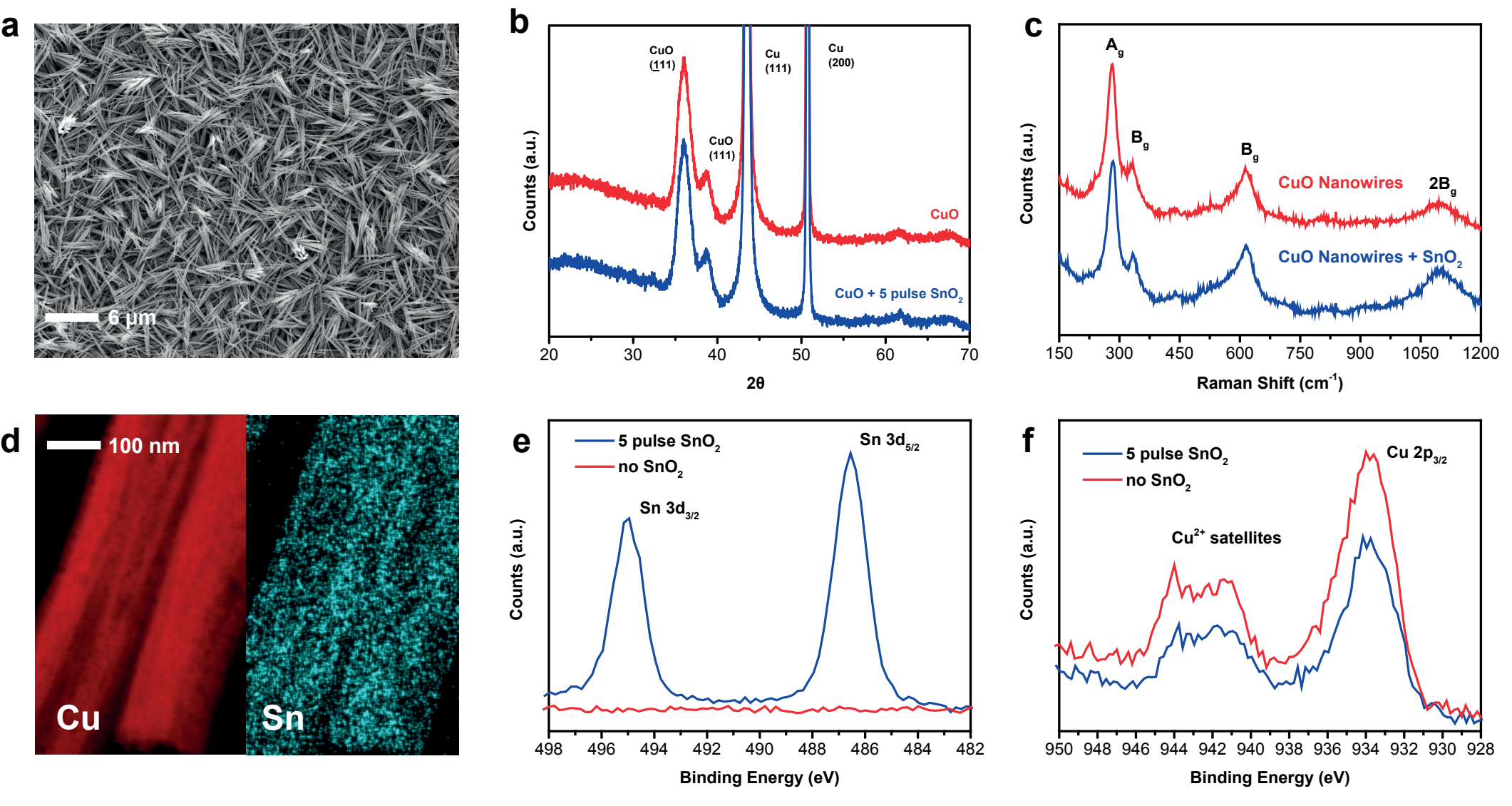
a
6 μm
b
CuO (111)
CuO (111)
Cu (111)
Cu (200)
CuO
CuO + 5 pulse SnO2
Counts (a.u.)
20 30 40 50 60 70
2θ
c
Ag
Bg
Bg
2Bg
CuO Nanowires
CuO Nanowires + SnO2
Counts (a.u.)
150 300 450 600 750 900 1050 1200
Raman Shift (cm-1)
d
100 nm
Cu
Sn
e
5 pulse SnO2
no SnO2
Sn 3d5/2
Sn 3d3/2
Counts (a.u.)
498 496 494 492 490 488 486 484 482
Binding Energy (eV)
f
5 pulse SnO2
no SnO2
Cu 2p3/2
Cu2+ satellites
Counts (a.u.)
950 948 946 944 942 940 938 936 934 932 930 928
Binding Energy (eV)

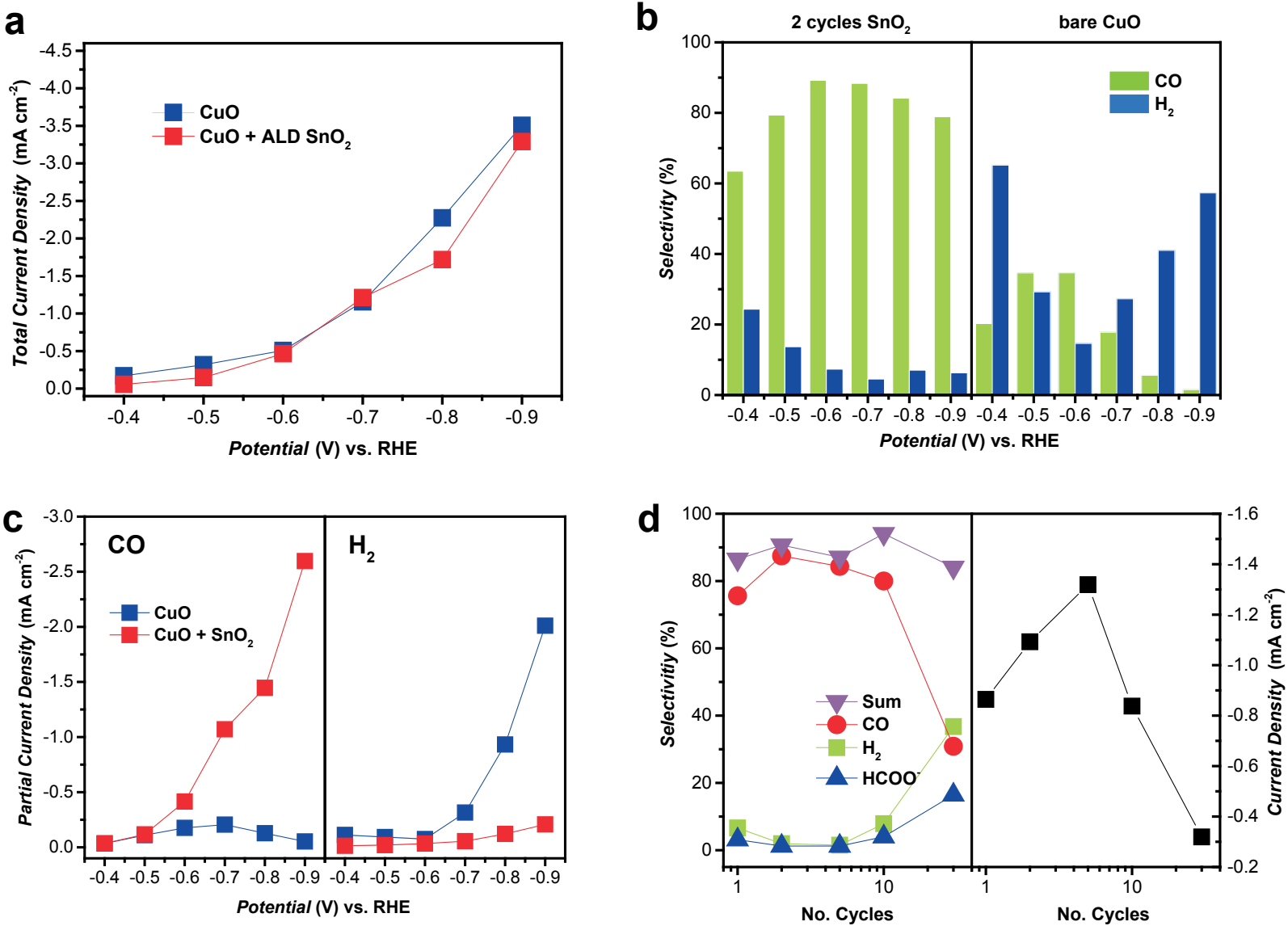
a
Total Current Density (mA cm-2)
CuO
CuO + ALD SnO2
Potential (V) vs. RHE
b
2 cycles SnO2
bare CuO
CO
H2
Selectivity (%)
Potential (V) vs. RHE
c
CO
H2
CuO
CuO + SnO2
Partial Current Density (mA cm-2)
Potential (V) vs. RHE
d
Selectivitiy (%)
Sum
CO
H2
HCOO-
No. Cycles
No. Cycles
Current Density (mA cm-2)

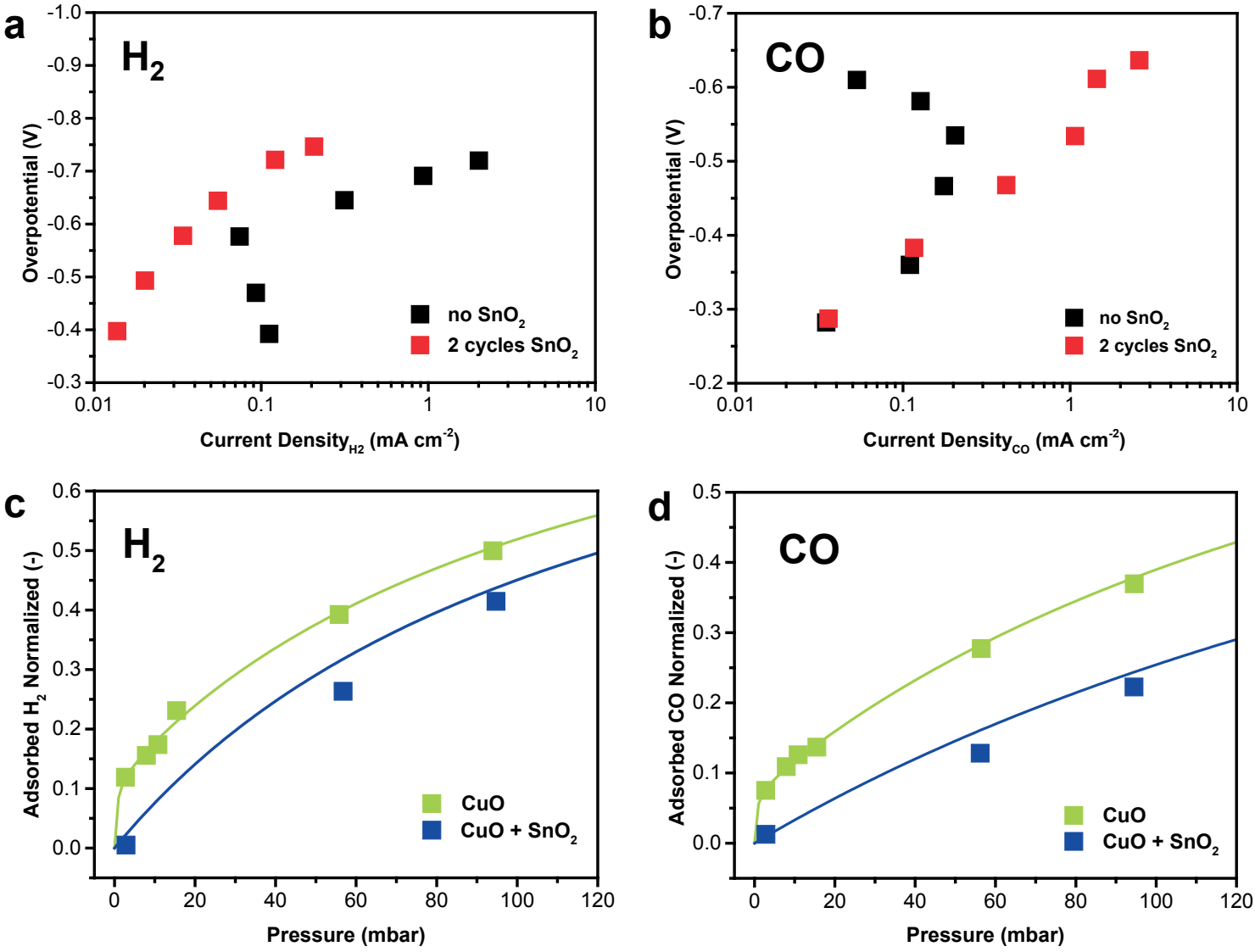
a
H2
Overpotential (V)
-1.0
-0.9
-0.8
-0.7
-0.6
-0.5
-0.4
-0.3
0.01
0.1
1
10
Current Density H2 (mA cm-2)
no SnO2
2 cycles SnO2
b
CO
Overpotential (V)
-0.7
-0.6
-0.5
-0.4
-0.3
-0.2
0.01
0.1
1
10
Current Density CO (mA cm-2)
no SnO2
2 cycles SnO2
c
H2
Adsorbed H2 Normalized (-)
0.6
0.5
0.4
0.3
0.2
0.1
0.0
0
20
40
60
80
100
120
Pressure (mbar)
CuO
CuO + SnO2
d
CO
Adsorbed CO Normalized (-)
0.5
0.4
0.3
0.2
0.1
0.0
0
20
40
60
80
100
120
Pressure (mbar)
CuO
CuO + SnO2

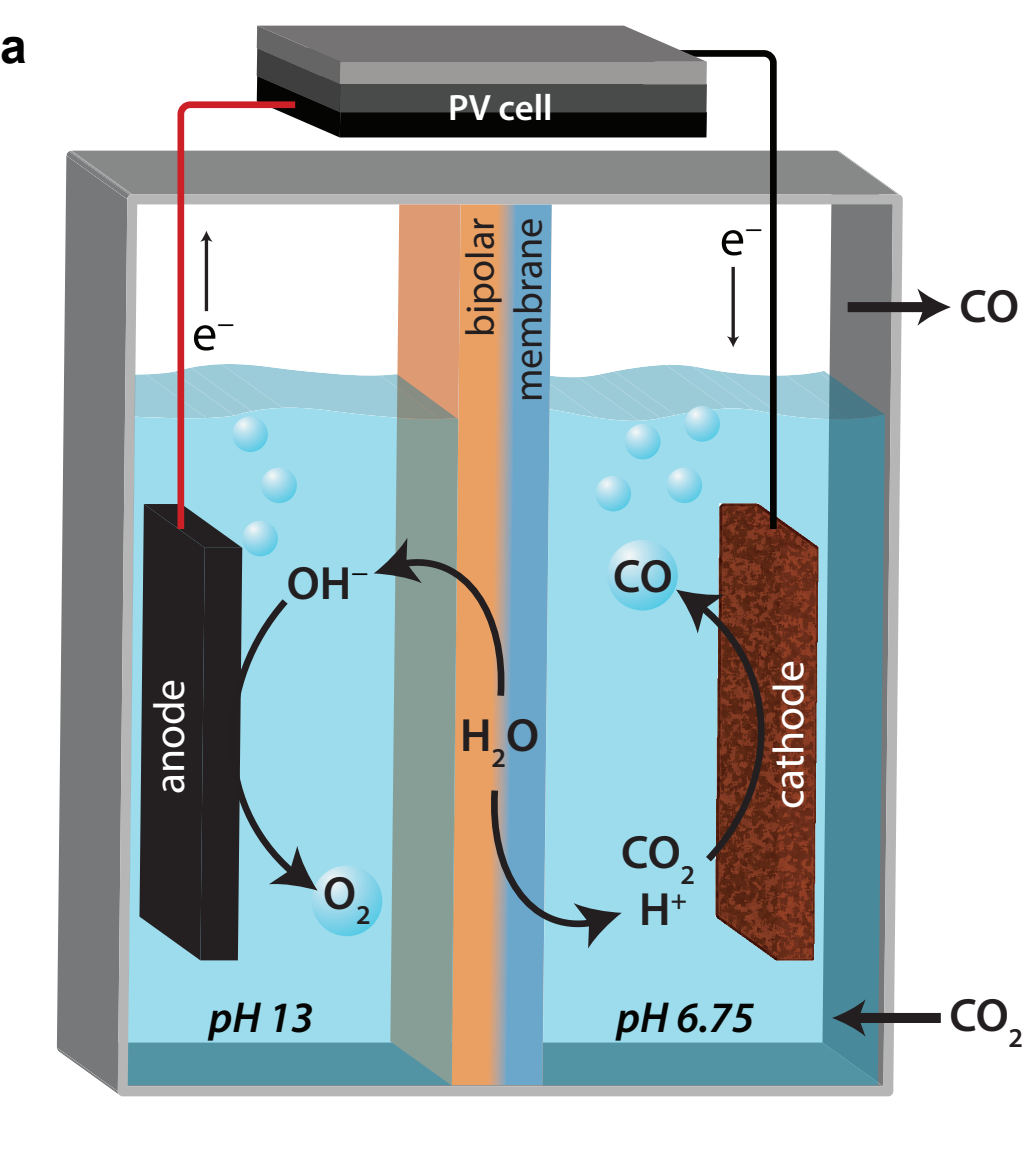
a
PV cell
e⁻
e⁻
bipolar membrane
CO
OH⁻
anode
CO
cathode
H₂O
CO₂
H⁺
O₂
pH 13
pH 6.75
CO₂

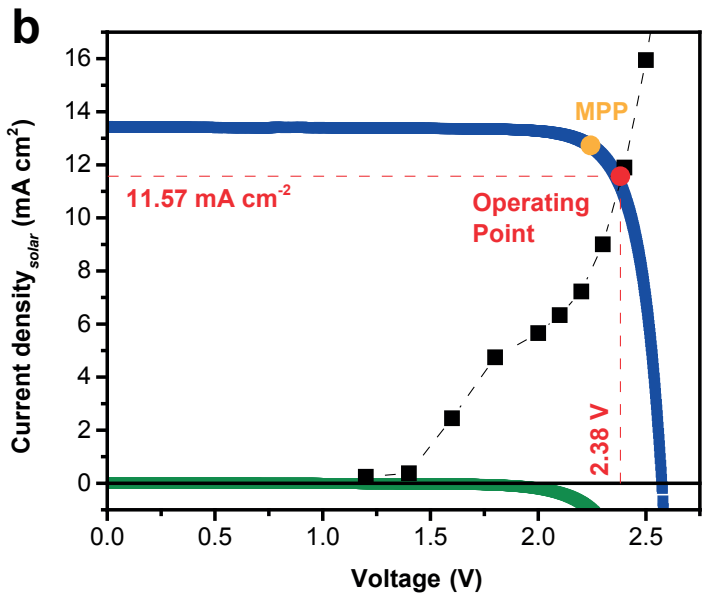
b
Current density$_{solar}$ (mA cm^{-2})
Voltage (V)
MPP
11.57 mA cm^{-2}
Operating Point
2.38 V

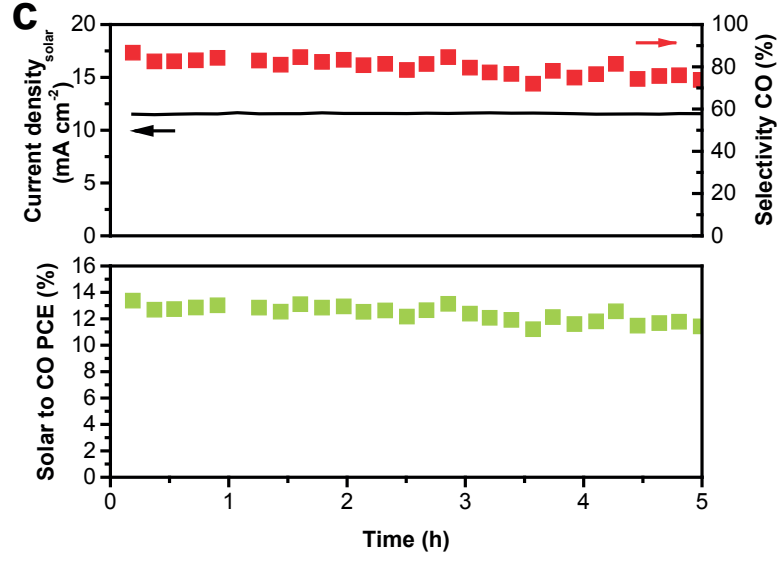
c
Current density$_{solar}$ (mA cm^{-2})
Selectivity CO (%)
Solar to CO PCE (%)
Time (h)